Supporting Information

Molecular-level Design and Green Process Engineering: Optimizing Pseudo-Graphitic Domains in Pitch-derived hard carbon for Fast Sodium Storage

Dan Zhao, Hanqing Zhao, Lingwei Kong, Shulian Lei, Boyan Cui, Tingjun Fu, and Zhong Li **

State Key Laboratory of Clean and Efficient Coal Utilization, College of Chemistry and Chemical Engineering, Taiyuan University of Technology, Taiyuan 030024, Shanxi, China

* Corresponding author.

E-mail address: zhaohanqing@tyut.edu.cn (H. Zhao) lizhong@tyut.edu.cn (Z. Li)

1. Materials and general methods

1.1 Synthesis of carbon materials

Coal tar pitch (CTP, softening point of 78.8 °C) was obtained from Ningxia Baichuan New materials Co., Ltd. The CTP was oxidized with the mixed solution of formic acid and hydrogen peroxide, specifically prepared as follows: A homogeneous mixture of 240 mL formic acid and 24 mL hydrogen peroxide was prepared, followed by the addition of 1.6 g of CTP. The oxidative cleavage reaction was carried out under continuous stirring at 25 °C for 20 h. The resulting mixture was transferred to a 50 mL centrifuge tube and separated by centrifugation at 10,000 rpm for 10 min. The supernatant was collected and concentrated using a rotary evaporator at 60 °C under reduced pressure (-0.08 MPa). The obtained product underwent purification through two cycles of dissolution-reprecipitation with absolute ethanol, yielding a yellowish-brown lightweight oxidation product (denoted as L-OCTP). Since the L-OCTP did not contain graphite nanodomains, it was also designated as NGC (N: none; G: graphite nanodomains; C: CTP). The precipitate at the bottom of the centrifuge tube was vacuum-filtered through a 0.22 μm microporous membrane and repeatedly washed until the filtrate was neutral. After vacuum drying at 60 °C for 12 h, a dark brown solid oxidation product (designated as S-OCTP) was obtained.

1.5 g of NGC was dissolved in 150 mL of deionized water, placed in Teflon. After sonicated for 30 min, an aqueous NGC solution with a concentration of 10 % was conFig.d. Then, it was hydrothermal treatment in an oven at 180 °C for 6 h. After cooling, the samples were washed with deionized water until the filtrate was colorless. Finally, the samples were obtained by drying overnight in vacuum oven at 60 °C, denoted as SGC (S: small). As the same process, LGC (L: large) was prepared, in which the concentration of NGC solution was 50%. Accordingly, the derived HC was obtained by carbonizing CTP, NGC, SGC, LGC, and S-OCTP in a tubular furnace at 1300 °C for 2 h with a heating rate of 5 °C min^{-1} in Ar atmosphere. The hard carbons were labeled as SC, NGC-HC, SGC-HC, LGC-HC, and S-OCTP-HC, respectively.

1.2 Materials Characterization

The morphologies and microstructures of the samples were investigated by Scanning Electron Microscopy (SEM, FEI-Quanta FEG 250) and Transmission Electron Microscopy (TEM, JEOL JEM-2100FMII). The carbonization of sample was detected via Thermogravimetric analysis (TGA). The elemental distribution of sample was tested with an energy dispersive spectrometer (EDS). To analyze the surface chemistry of the samples, X-ray Photoelectron Spectroscopy (XPS, Thermo Fisher Scientific Escalab 250Xi) and Fourier Transform Infrared Spectra (FTIR, Bruker Invenio s) were used. The structure property of CTP precursor was detected by Wide cavity solid state nuclear magnetic spectrometer (^{13}C NMR, AVANCE IIITM 600 MHz). The closed pore structure of sample was determined by synchrotron radiation SAXS-WAXS techniques (Beijing Synchrotron Radiation Facility:1W2A). N_2 adsorption-desorption was carried out at Beishide 3H-200PS2 instrument at -196 °C. The X-ray diffraction (XRD) characterization was carried out to analysis the crystal structure of CTP precursor and derived HC, and structure change of in-situ discharge/charge process on Rigaku SmartLab SE diffractometer using Cu Kα radiation source (λ = 0.154056 nm, θ = 10-80°). Raman and ex/in-situ Raman spectra were recorded by a Renishaw Invia Reflex (laser: 514 nm).

1.3 Electrochemical Measurements

In a glove box, the half-cells were assembled using 2025-type coin cell, where sodium piece as counter electrode, a glass fiber membrane as separator. The anode slurry was obtained by mixing the active materials, Super P, and poly(vinylidene fluoride) (PVDF) at the mass ratio of 7:2:1 in N-methyl-2-pyrrolidone (NMP). Then, the slurry was uniformly spread on copper foil by an applicator (100 μm). Vacuum dried at 100 °C overnight, the electrode sheets were received with a loading mass of active materials about 1.0 mg cm^{-2}. $NaPF_6$ (1M) dissolved into 100% DME as the electrolyte. $Na_3V_2(PO_4)_3$@C (NVP@C), Super P, and PVDF were mixed in NMP with a mass ratio of 8:1:1, and coated evenly on an aluminum foil. Then, it was assembled with SGC-HC anode sheet into a full-cell. The separator was the same as the half cells. The electrolyte was 1 M $NaClO_4$ in ethylene carbonate (EC) and propylene carbonate (PC) (1:1, vol/vol) with 5 wt% fluoroethylene carbonate (FEC).

The galvanostatic charge/discharge, rate capability, long-term cycle stability, and galvanostatic intermittent titration technique (GITT) were characterized on LAND 2001A apparatus in a voltage range of 0.01-3.0 V. Cyclic voltammetry (CV) profiles and electrochemical impedance spectra (EIS) were performed at the CHI1000C and CHI660E workstation, respectively.

2. Supplementary Fig.S and Table S

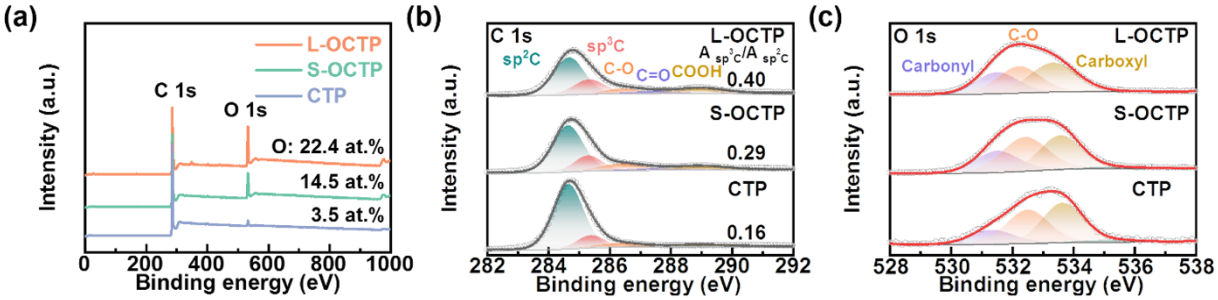

Fig. S1 (a) The full XPS spectra and high-resolution XPS spectra of (b) C1s and (c) O 1s of OCTP samples.

The C 1s XPS spectra of the sample (Fig. S1b) are divided into sp^2 C, sp^3C, C-O, C=O, and COOH peaks at binding energies of 284.6, 285.3, 286.4, 287.4, and 288.9 eV, respectively. In the O 1s XPS spectrum of the sample (Fig. S1c), peaks corresponding to carbonyl, C-O, and carboxyl are observed at 531.5, 532.5, and 533.7 eV, respectively.

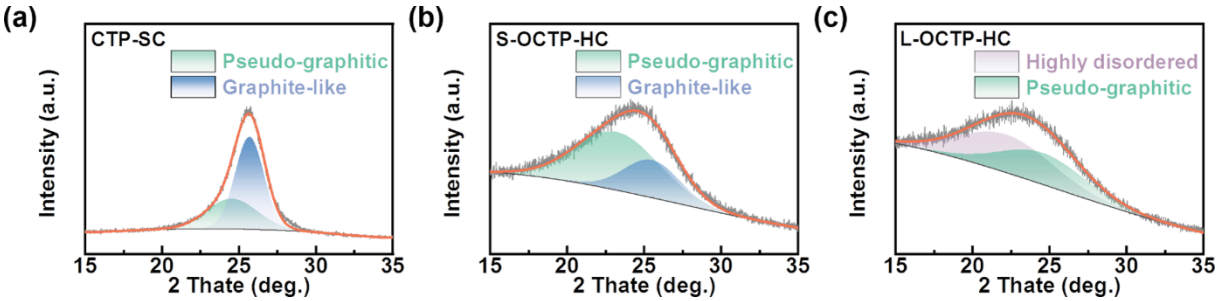

Fig. S2 The XRD patterns and the fitted results of C (002) diffraction peak for (a) CTP-SC, (b) S-OCTP-HC, and (c) L-OCTP-HC.

As shown in Fig. S2a-c, the (002) peak can be fitted into three crystalline types based on the interlayer spacing: highly disordered carbon (> 0.4 nm), pseudo-graphitic nanodomain (0.36~0.4 nm), and graphite-like nanodomain (< 0.36 nm). The position and proportion of these three crystalline types were listed in Table S1.

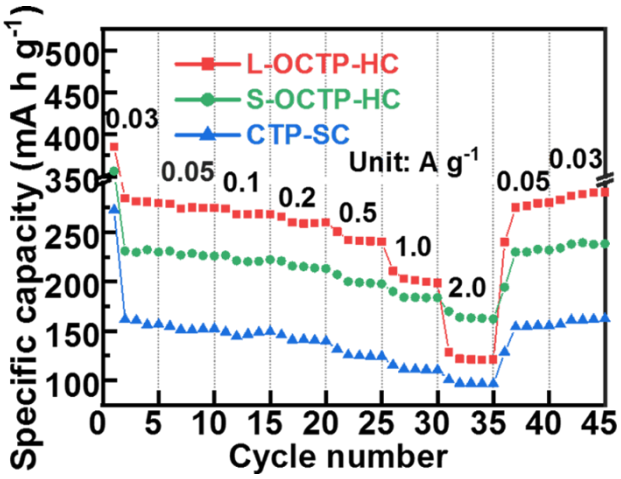

Fig. S3 Rate performance from 0.03 A g^{-1} to 2 A g^{-1}.

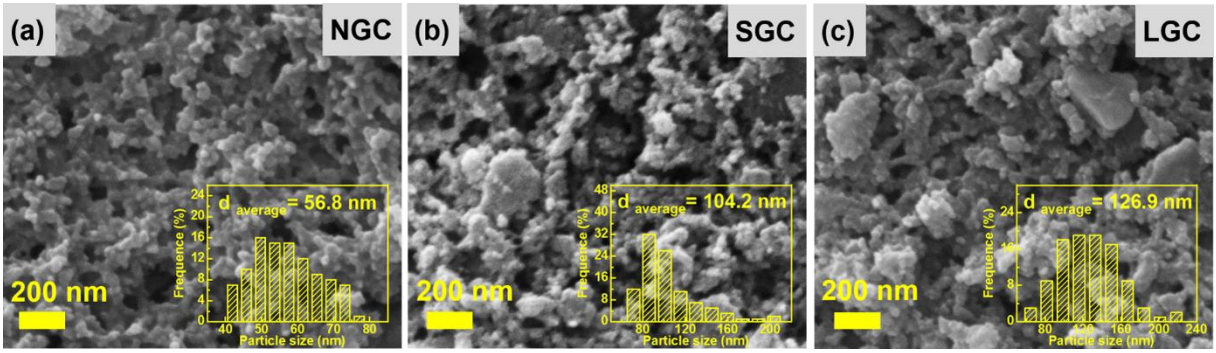

Fig. S4 (a-c) SEM images of NGC, SGC, and LGC.

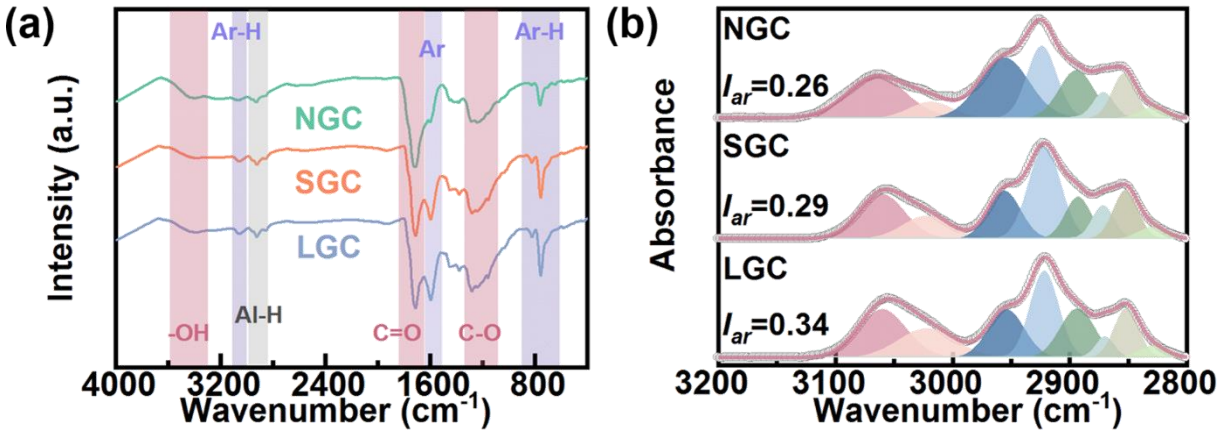

Fig. S5 The FTIR curves and (b) the fitted curves of FTIR in the range of 3200-2800 cm^{-1} of NGC, SGC, and LGC.

In Fig. S5a, the FTIR spectra of all samples show the -OH stretching vibration band at approximately 3418 cm^{-1}, the C=O stretching vibration band at 1710 cm^{-1}, and the C-O stretching bands at 800-1200 cm^{-1}. Other peaks appear in the purple region at 3100-2980 cm^{-1}, 1600, and 700-900 cm^{-1}, belonging to the sp^2 aromatic C-H stretching bond (Ar-H). The peaks in the grey region of 2980-2830 cm^{-1} are attributed to the sp^3 aliphatic C-H (Al-H) stretching bond. The aromaticity index (I_{ar}), reflecting the content of aromatic components in the material, can be calculated by fitting the peaks at 3100-2800 cm^{-1} (in Fig. S5b). Among them, the peaks at around 3060 and 3020 cm^{-1} belong to aromatic C-H stretching bands, and the remaining five peaks at 2954, 2921, 2893, 2870, 2852, and 2830 cm^{-1} are ascribed to the vibration of aliphatic hydrogen.

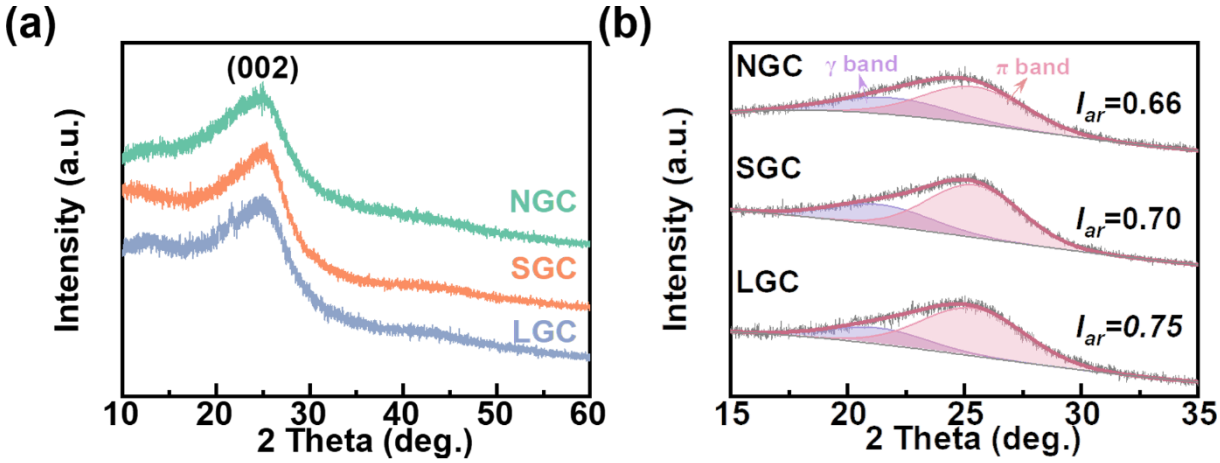

Fig. S6 (a)The XRD patterns and (b) the fitted curves about C (002) peak.

The XRD patterns (Fig. 1e and S6) of samples exhibit an obvious diffraction peak located at around 26°, corresponding to the (002) lattice plane of carbon.

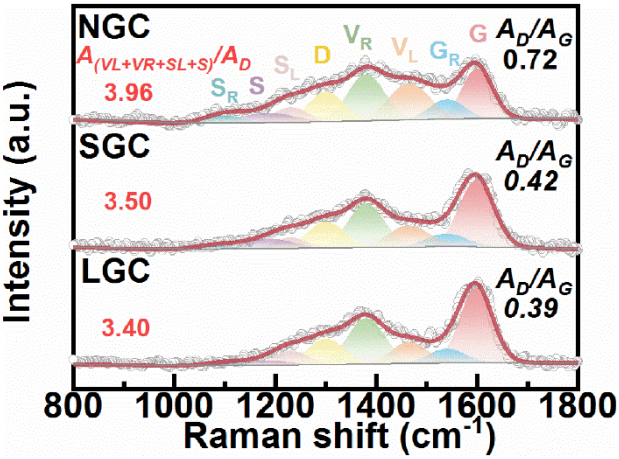

Fig. S7 The Raman spectra of NGC-HC, SGC-HC, and LGC-HC.

Raman spectra of all samples display two main peaks centered at 1350 and 1585 cm^{-1}, which are related to the disorder-induced D-bands and in-plane vibrational G-bands, respectively (Fig. S7). Commonly, the area ratio of D and G peaks (A_D/A_G) can reflect the disorder degree of carbon.

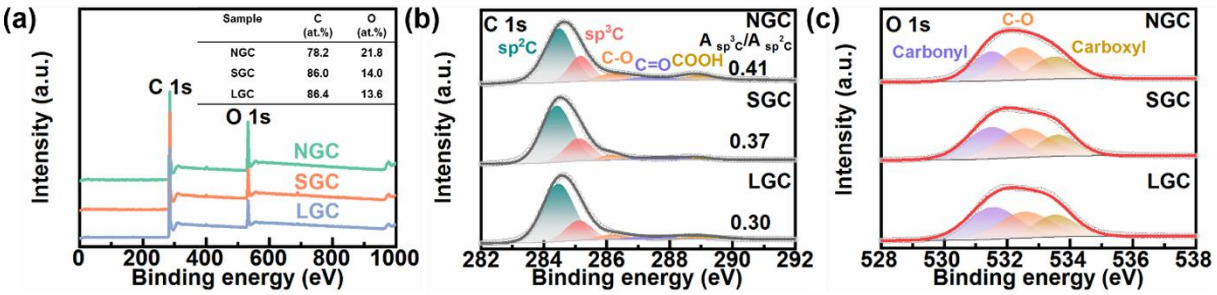

Fig. S8 (a) The full XPS spectra and high-resolution XPS spectra of (b) C1s and (c) O 1s of all samples.

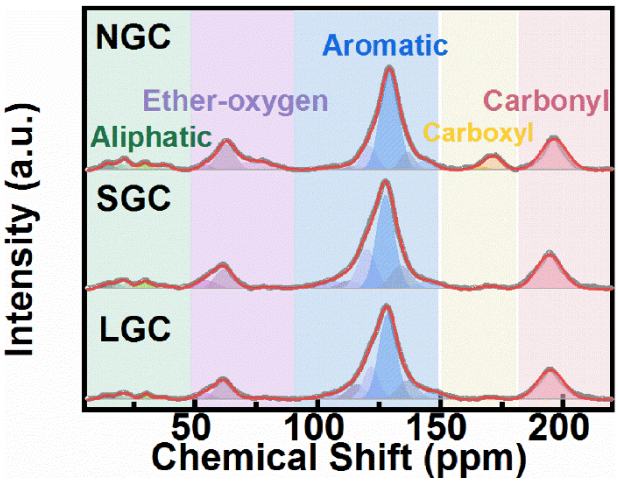

Fig. S9 The fitted curves of ^{13}C NMR spectra.

Generally, all samples can be roughly divided into four carbon atom types, namely aliphatic carbon at 0~50 ppm, ethoxy carbon at 50~90 ppm, aromatic carbon at 90~165 ppm, and the carbon atoms of carbonyl and carboxyl groups at 165~220 ppm.

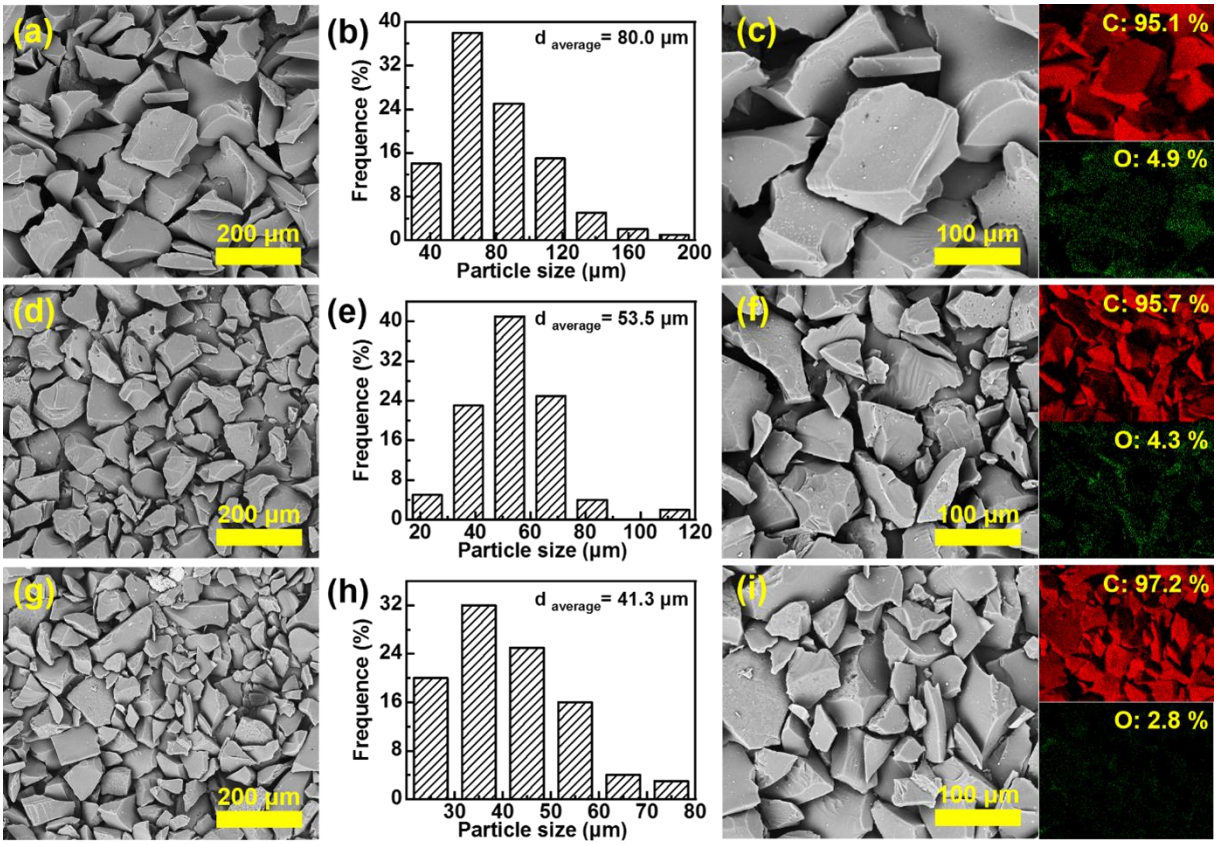

Fig. S10 SEM-EDS images and the distribution of particle size for (a-c) NGC-HC, (d-f) SGC-HC, and (g-i) LGC-HC.

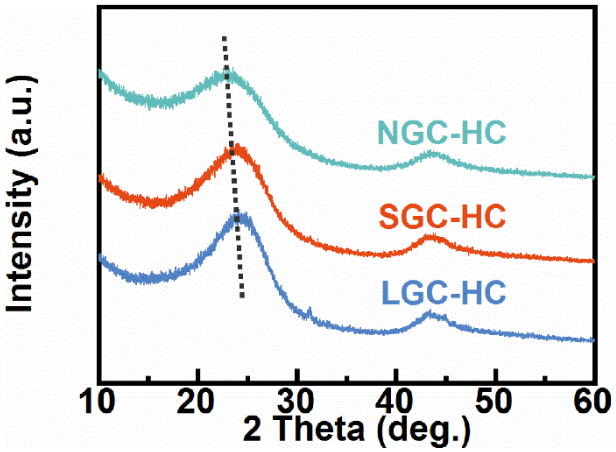

Fig. S11 The XRD patterns of NGC-HC, SGC-HC, and LGC-HC.

The XRD patterns (Fig. 1e) of samples exhibit an obvious diffraction peak located at around 26°, corresponding to the (002) lattice plane of carbon, and C (100) peak at around 42.5°. The parameter (R), a representative measure calculated from the intensity of the (002) peak, which represents the ratio of the peak height to the background, has been used to quantify the degree of carbon disorder.

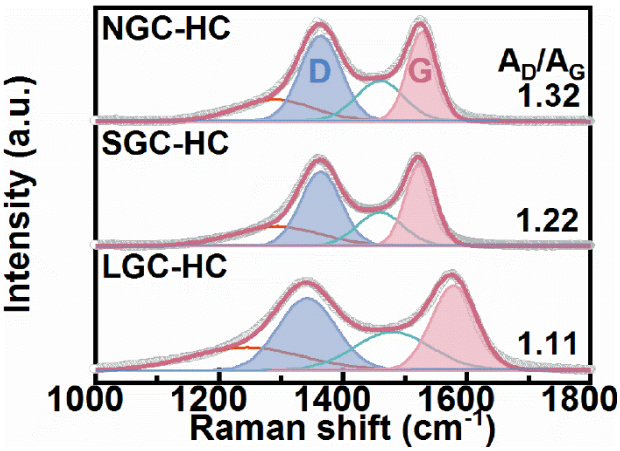

Fig. S12 The Raman spectra of NGC-HC, SGC-HC, and LGC-HC.

Raman spectra of all samples display two main peaks centered at 1350 and 1585 cm^{-1}, which are related to the disorder-induced D-bands and in-plane vibrational G-bands, respectively. Commonly, the area ratio of D and G peaks (A_D/A_G) can reflect the disorder degree of carbon.

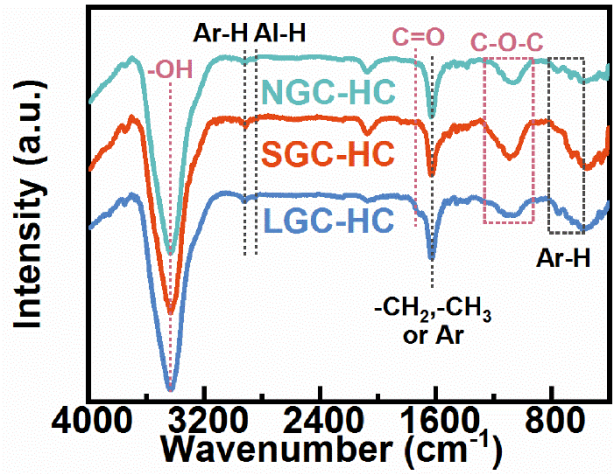

Fig. S13 The FTIR spectra of NGC-HC, SGC-HC, and LGC-HC.

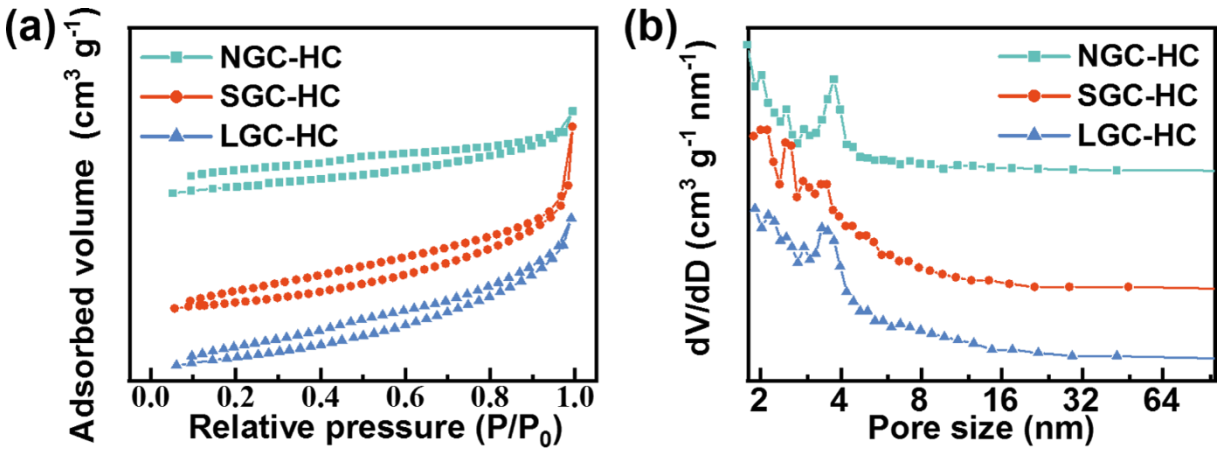

Fig. S14 (a) The N_2 adsorption-desorption isotherms and (b) the pore size distribution of the sample.

The specific surface area was calculated using the Brunauer-Emmett-Teller (BET) method. The mesoporous and micropore pore size distribution of the samples was obtained by the Barrett-Joyner-Halenda (BJH) model and T-Plot model.

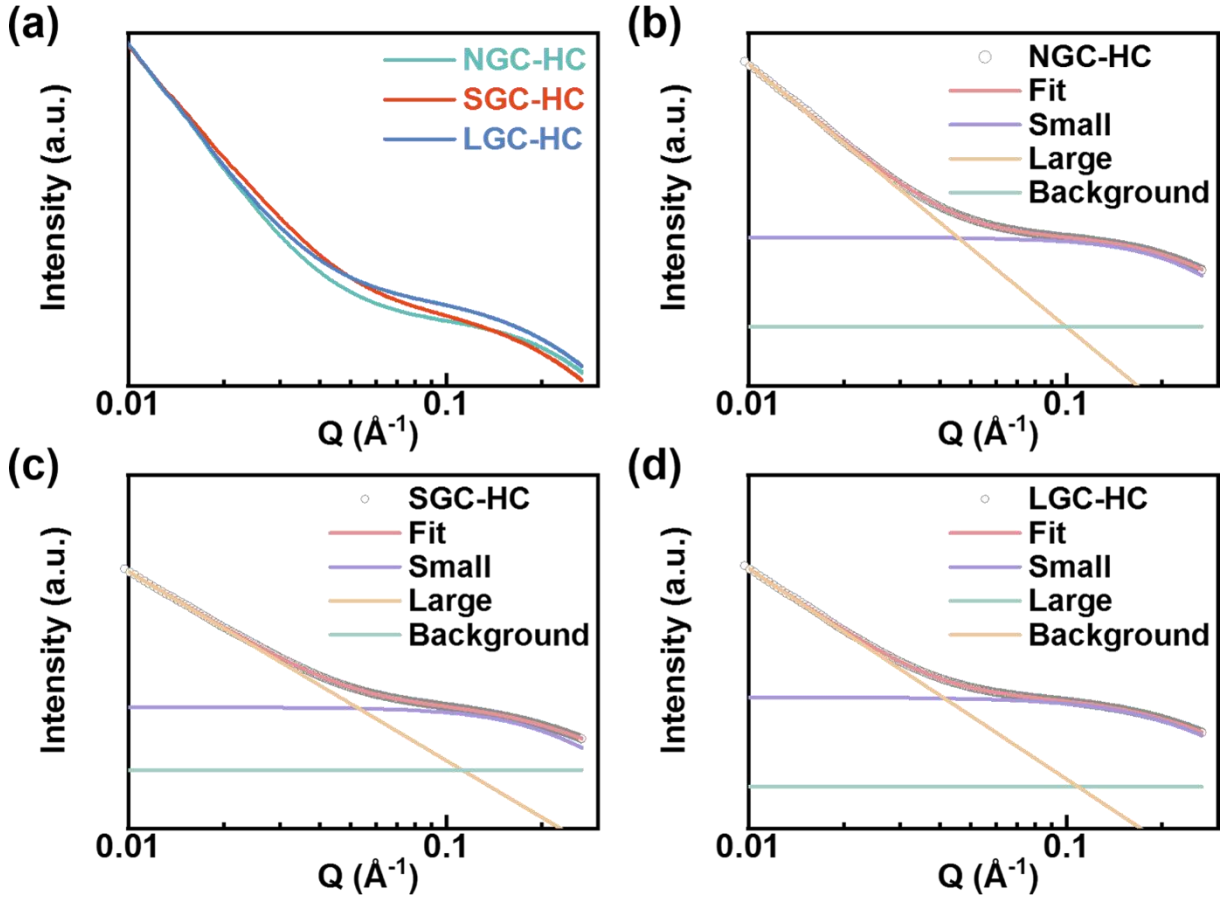

Fig. S15 (a) SAXS patterns and (b-d) fitting curve of SAXS patterns presenting pores of the sample.

The closed pore structure of sample was determined by synchrotron radiation SAXS-WAXS techniques (Beijing Synchrotron Radiation Facility:1W2A). The X-ray with 0.154 nm was injected into 1W2A beamline and the beam spot with 1.4 × 0.2 mm was set on Pilatus 2MF detector. The samples were placed at 1834 mm far from SAXS detector. The two-dimension images were recorded with an exposure time of 2 s.

The SLD Cacalator of Sasfit software was used to calculate the scattering length density (SLD) of the carbon materials. According to the following formula, the structure density (ρ_{struct}) of the carbon materials was calculated by using the structural parameters:

$$\rho_{struct} = \rho_{graphite} \frac{d_{002}^{graphite}}{d_{002}} \left(\frac{d_{100}^{graphite}}{d_{100}}\right)^2 \quad \text{(Equ. 1)}$$

Where $\rho_{graphite}$ is the structural density of graphite. 2.26 g cm^{-3}, d_{002} and $d_{002}^{graphite}$ is the interlayer distance of the sample and of graphite respectively. d_{001} and $d_{001}^{graphite}$ is the in-plane distance of the sample and of graphite respectively, as shown in Equ. 1.

The micropores of HC can be modelized by the semi-empirical Teubner-Strey model.

$$I_{mp} = I_0 \frac{1}{1+C_1Q^2+C_2Q^4} \quad \text{(Equ. 2)}$$

I_0, C_1 and C_2 can be calculated by following equation:

$$I_0 = \frac{8\pi}{\rho_{struct}} \emptyset(\Delta SLD)^2 \frac{\xi^3}{(1+(\frac{2\pi\xi}{d})^2)^2} \quad \text{(Equ. 3)}$$

The d is the pore-pore distance and ξ is a correlation length that limits the extension of the order (Equ. 4 and 5) which were calculated from SasView software by fitting SAXS data. C_1 was calculated from the d and ξ, then the closed pore diameter of the sample was calculated by Equ. 6.

$$d = 2\pi \left[\frac{1}{2} C_2^{-\frac{1}{2}} - \frac{C_1}{4C_2}\right]^{-\frac{1}{2}} \quad \text{(Equ. 4)}$$

$$\xi = \left[\frac{1}{2} C_2^{-\frac{1}{2}} + \frac{C_1}{4C_2}\right]^{-\frac{1}{2}} \quad \text{(Equ. 5)}$$

$$r = \sqrt{5C_1} \quad \text{(Equ. 6)}$$

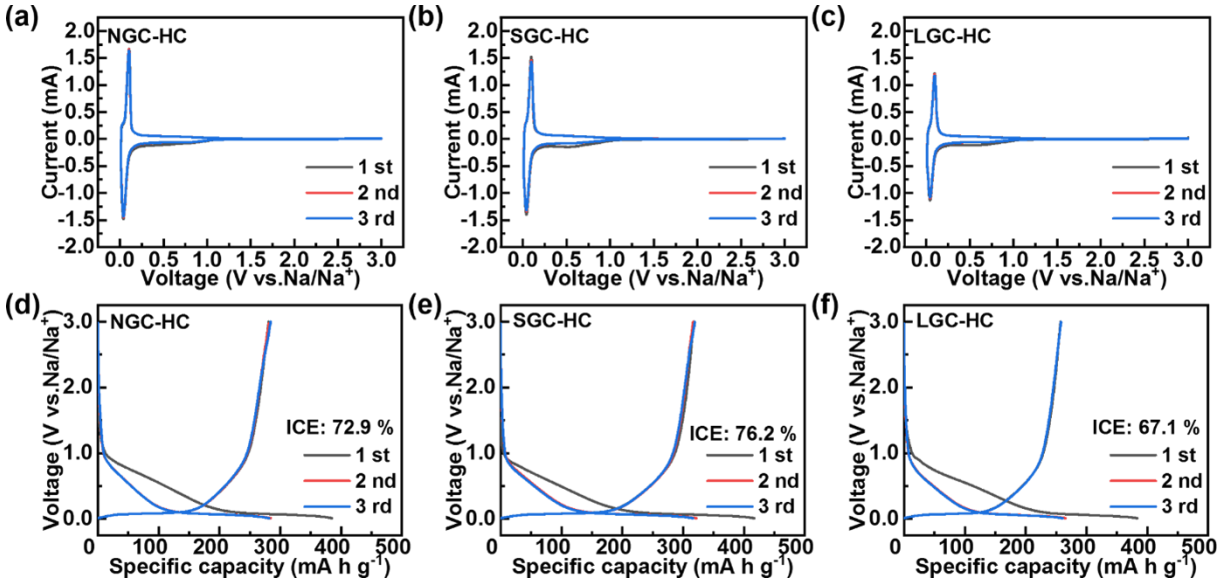

Fig. S16 (a-c) The CV curves in the initial three cycles and (d-f) galvanostatic charge/discharge curves at a current density of 0.03 A g^{-1}.

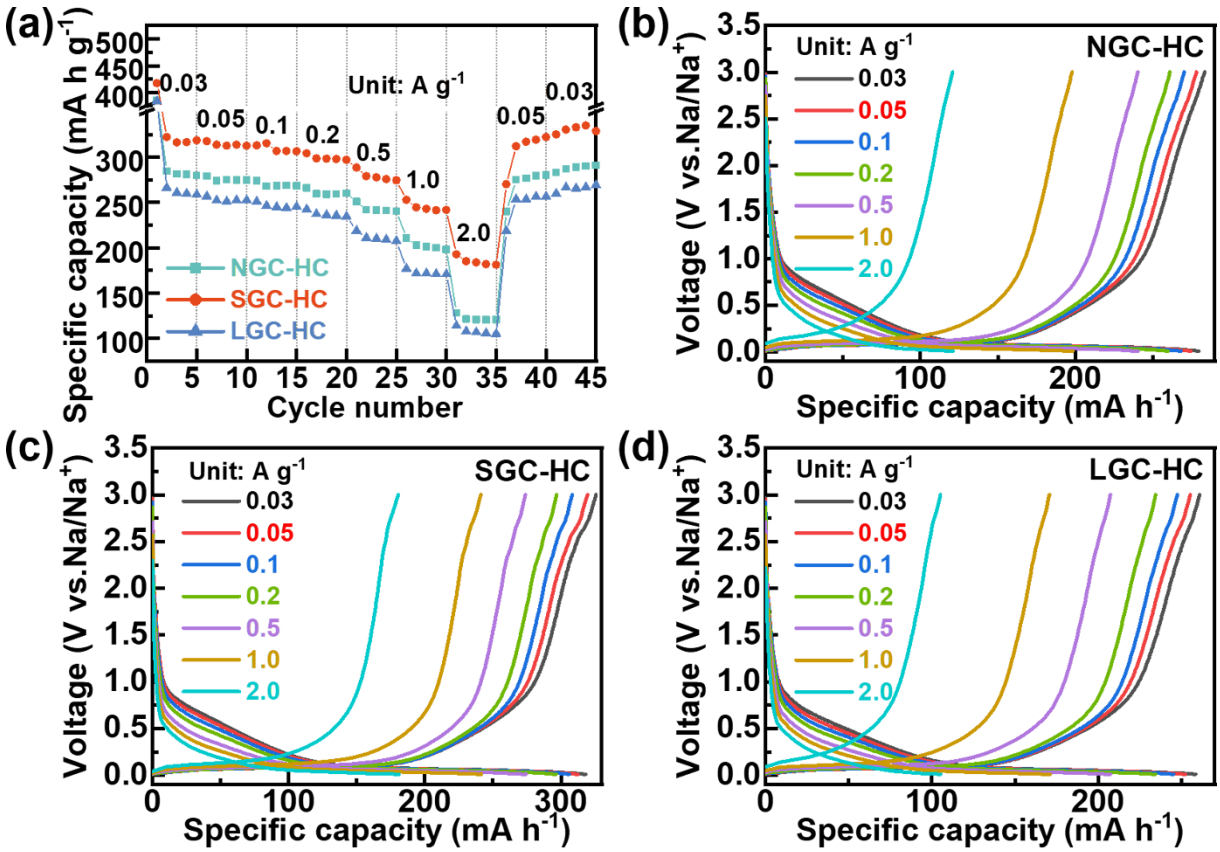

Fig. S17 (a) The rate performance, (b) galvanostatic charge/discharge curves at different rates of the sample.

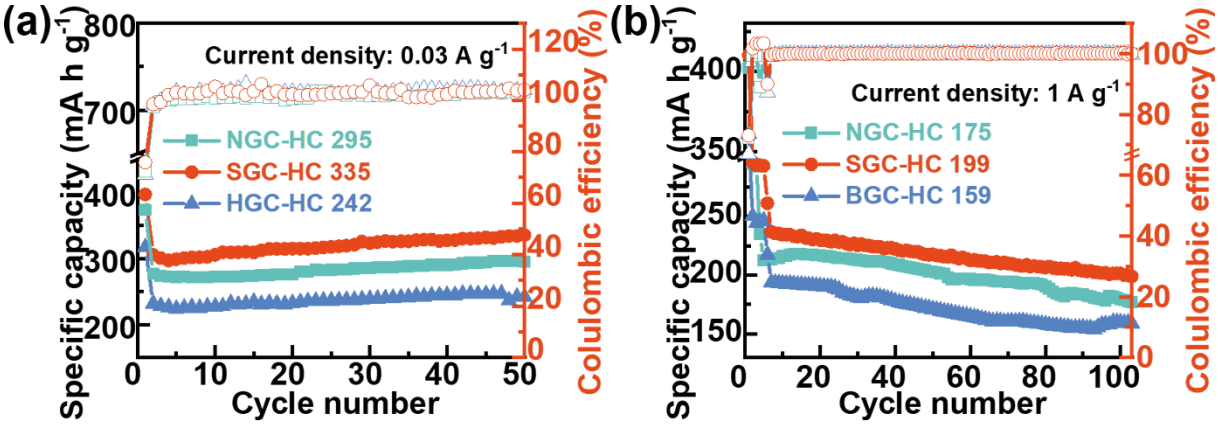

Fig. S18 The cycling stability at (c) 0.03 and (d)1 A g^{-1}.

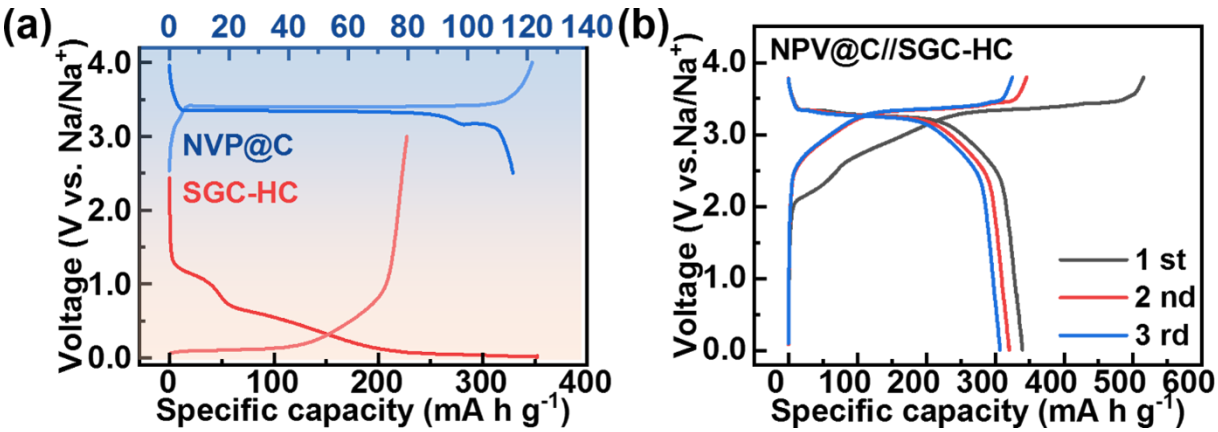

Fig. S19 Galvanostatic charge/discharge curves of (a) SGC-HC and NVP@C half-cell in the first cycle at 0.03 A g^{-1}, (b) NVP@C//SGC-HC in the initial three cycles at a current density of 0.03 A g^{-1}.

The capacity ratio of the negative to positive electrodes (N/P) is controlled at 1.2 to maximize the energy density and reinforce the stability of the Na-ion full cells. And the capacities are normalized by the active mass of the anode.

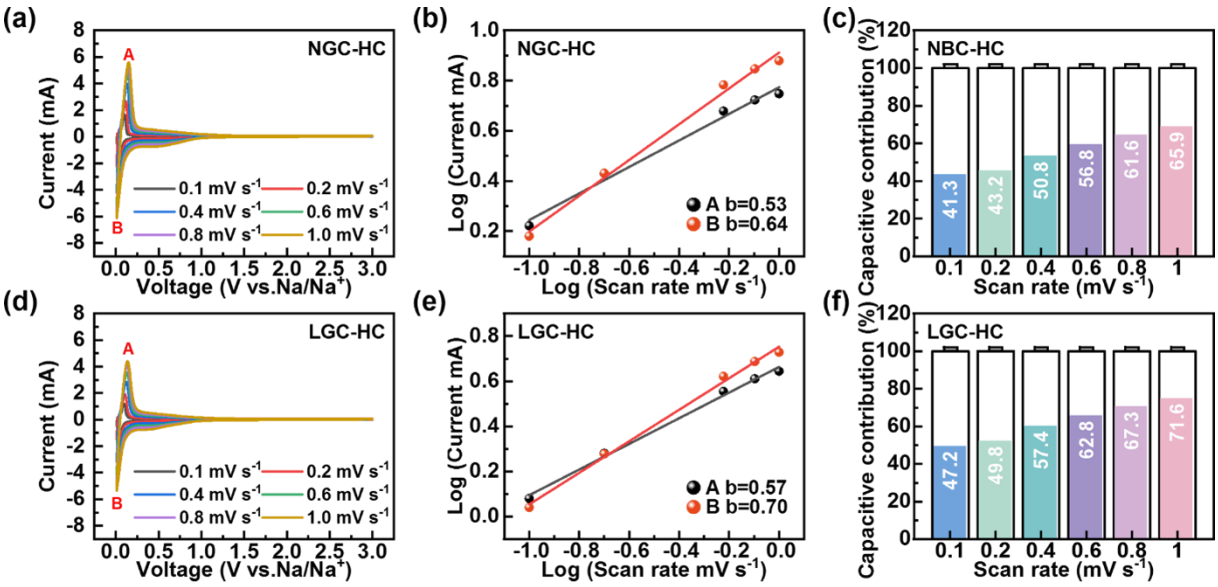

Fig. S20 (a,d) CV curves, (b,e) the linear correlation between log(i) and log (v), and (c,f) capacitive contribution of NGC-HC and LGC-HC, respectively.

The peak current (*i*) and scan rate (*v*) obey the power-law relationship as follows:

$$i = av^b$$

$$log\ (i) = b\ log\ (v) + a \qquad \text{(Eqn. 7)}$$

where *a* and *b* are constants. The *b* value can be calculated by fitting the log(*i*)-log(*v*), and the results are shown in Fig. 6b and S20b,e. When *b* value approaches 0.5, the Na storage is dominated by a diffusion-controlled process, while 1.0 means the electrochemical process is mainly controlled by a pseudo-capacitive process.

The pseudo-capacitive contribution (k_1v) and diffusion-controlled contribution ($k_2v^{1/2}$) were quantitatively calculated by the formula as

$$i = k_1 v + k_2 v^{1/2} \quad \text{(Eqn. 8)}$$

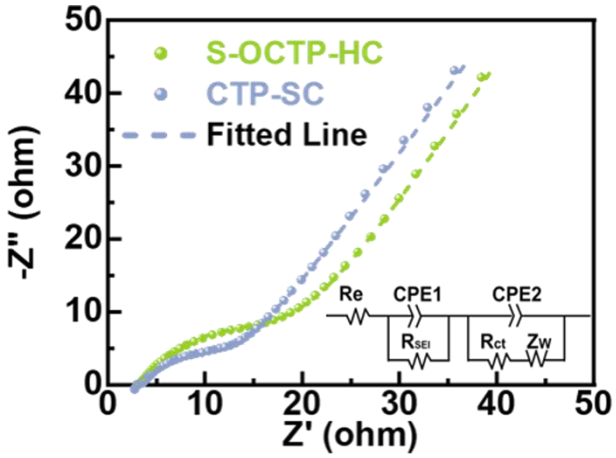

Fig. S21 The Nyquist plots and the fitted results via the equivalent circuit diagram.

An equivalent circuit model was proposed to fit the EIS results, and the results are exhibited in Fig. 6d and Table S9. The curves are well-fitted with small chi-square values (less than 10^{-3}). In the equivalent circuit model (Fig. S21), R_e includes the self-resistance of electrolyte and electrode, the interface contact resistance of the current collector and electrode material, R_{SEI} stands for the resistance of Na^+ through SEI film, R_{ct} represents the charge transfer resistance that related to the electrochemical reaction, CPE is considered as an imperfect capacitor, Z_w is diffused Warburg impedance owing to the Na^+ diffusion inside of material.

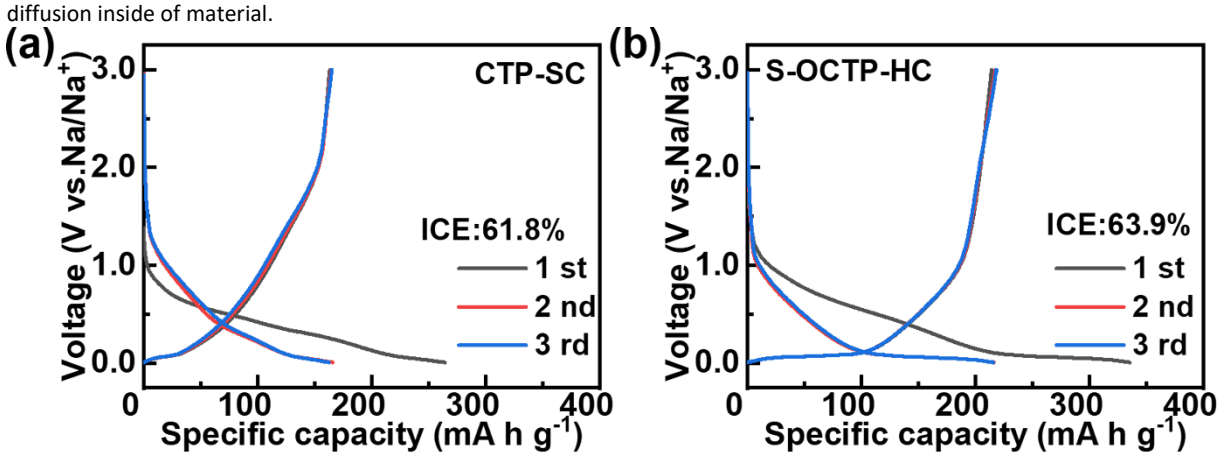

Fig. S22 The galvanostatic charge/discharge curves at a current density of 0.03 A g^{-1}.

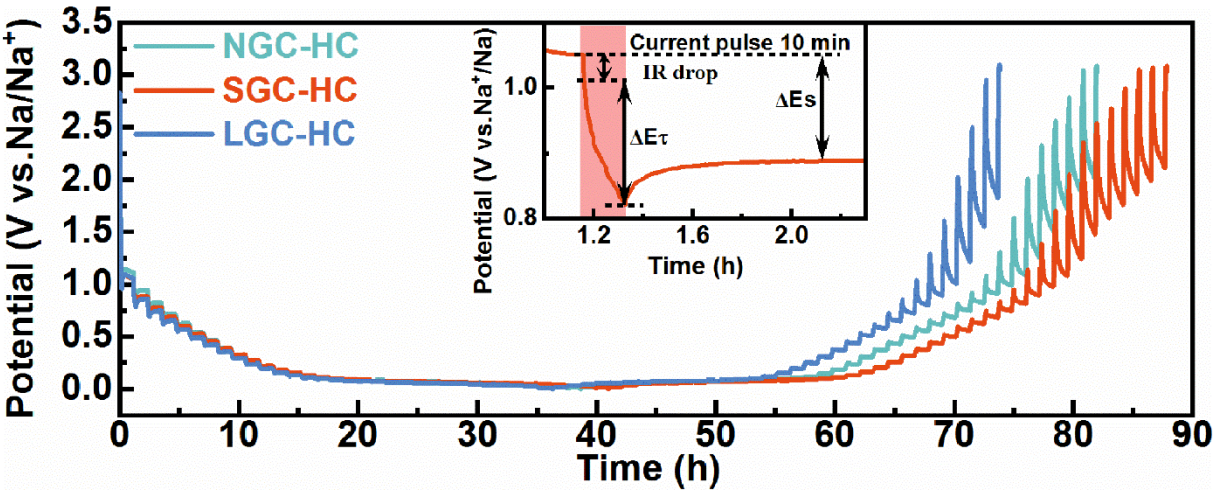

Fig. S23. GITT curves (inset: calculation method of *ΔEs* and *ΔEτ* about the single GITT titration curve).

The LAND 2001A apparatus also was applied to analyse the diffusion coefficient of Na^+ using the galvanostatic intermittent titration technique (GITT) (current pulse: 0.1 A g^{-1}, duration time: 10 min, relaxation time: 1 h). Fig. S23 displays the GITT curves of all samples in the second cycle with a pulse current of 0.03 A g^{-1}. The diffusion coefficients of Na^+ (D_{Na^+}) are calculated by Fick's second law and equation as follows:

$$D_{Na^+} = \frac{4}{\pi\tau}\left(\frac{m_B V_M}{M_b S}\right)^2\left(\frac{\Delta E_s}{\Delta E_\tau}\right)^2 \qquad \text{(Eqn. 9)}$$

Here τ is the current pulse time (s), M_b, V_M, and m_B are the molecular weights (g/mol), molar volume (cm^3/mol), and mass of the active material (g), respectively, S is the explored area (cm^2), L is the thickness (cm) of the electrode, ΔE_s and ΔE_τ (inset of Fig. S21) are the change in steady-state voltage and cell voltage, respectively.

Table S1 Textural parameters and fitted results of the samples by XRD.

Sample	d_{002} (nm)	L_a (nm)	L_c (nm)	Highly disordered		Pseudo-graphitic		Graphite-like	
				2 θ (°)	Area (%)	2 θ (°)	Area (%)	2 θ (°)	Area (%)
CTP-SC	0.354	8.78	3.09	-	-	24.6	36	25.7	64
S-OCTP-HC	0.379	6.66	1.54	-	-	23.2	70	25.5	30
L-OCTP-HC	0.385	6.19	1.28	22.2	57	24.6	43		

Table S2 Peak assigned for 8 sub-peaks of Raman spectra.

Band name	Position	Description
G	1598	graphite E^2_{2g}, aromatic ring quadrant breathing, alkene C=C
G_R	1540	aromatics with 3-5 rings, amorphous carbon structures
V_L	1465	methylene or methyl, semicircle breathing of aromatic rings, amorphous carbon structures
V_R	1380	methyl group, semicircle breathing of aromatic rings, amorphous carbon structures
D	1300	D band on highly ordered carbonaceous materials, C-C between aromatic rings and aromatics with no less than six rings
S_L	1230	aryl-alkyl ether, para-aromatics
S	1185	$C_{aromatic}$-C_{alkyl}, aromatic (aliphatic) ethers, C-C on hydroaromatic rings, hexagonal diamond carbon sp^3, C-H on aromatic rings
S_R	1080	C-H on aromatic rings, benzene (ortho-disubstituted) ring

Table S3 The elemental composition of samples based on XPS spectroscopy fitting.

Sample	C 1s (at.%)			O 1s (at.%)		
	sp^2C	sp^3C	$Asp^2C/A\ sp^3C$	Carbonyl	C-O	Carboxyl
NGC	55.3	22.5	0.41	31.8	41.1	27.1
SGC	63.8	23.3	0.37	40.1	38.7	21.2
LGC	64.1	19	0.30	41.6	34.8	23.6

Table S4 The structure attribution of chemical shifts based on ^{13}C NMR spectra.

Chemical Shift	Carbon type	Sign			
0-16	R-CH_3	f_{al}^{*}: –CH_3		f_{al}: total aliphatic carbon	
16-20	Ar-CH_3				
20-23	CH_2-CH_3				
23-35	CH_2	f_{al}^{H}: –CH or –CH_2			
35-50	C, CH				
50-60	O-CH_3, O-CH	f_{al}^{O}: bonded to oxygen			
60-75	O-CH				
75-90	R-O-R				
90-129	Ar-H	f_a^{H} : protonated aromatic			
129-137	Bridgehead (C-C)	f_a^{B}: aromatic bridgehead carbon	f_a^{N}: nonprotonated aromatic	f_a': aromatic carbon	f_a: total sp^2 carbon
137-150	Ar-C	f_a^{S}: alkylated aromatic carbon			
150-170	Ar-O	f_a^{P}: aromatic ether or phenolic hydroxylcarbon			
170-190	COOH	f_a^{c}: carbonyl or carboxyl carbon			
190-220	C=O				

Aliphatic carbons (f_{al}) are present on the side chains of aromatic hydrocarbon structural units, including methyl groups (f_{al}^{*}), quaternary and methylene groups (f_{al}^{H}), and oxygen-linked aliphatic carbons (f_{al}^{O}). sp^2 C is mainly composed of carbonyl carbon (f_a^{c}) and aromatic carbon (f_a'), while f_a' is composed of protonated aromatic (f_a^{H}) and nonprotonated aromatic carbon (f_a^{N}), among which f_a^{N} includes aromatic bridgehead carbon (f_a^{B}), alkylated aromatic carbon (f_a^{S}), and aromatic ether or phenolic hydroxylcarbon (f_a^{P}).

Table S5 The structure parameters of samples based on ^{13}C NMR spectroscopy fitting.

Sample	f_a	f_a^{c}	f_a'	f_a^{H}	f_a^{N}	f_a^{B}	f_a^{S}	f_a^{P}	f_{al}	f_{al}^{*}	f_{al}^{H}	f_{al}^{O}
NGC	75.7	19.7	56.0	10.4	45.6	35.5	8.9	1.2	24.3	4.1	3.2	17.1
SGC	82.7	16.3	66.4	21.5	44.9	31.7	12.6	0.7	17.3	3.2	2.8	11.4
LGC	85.1	17.1	68.0	21.6	46.4	34.0	12.2	0.2	14.9	2.8	1.6	10.5

f_a: total sp^2 carbon; f_a^{c}: carbonyl or carboxyl carbon; f_a': aromatic carbon; f_a^{H} : protonated aromatic carbon f_a^{N} : nonprotonated aromatic carbon; f_a^{B}: aromatic bridgehead carbon; f_a^{S}: alkylated aromatic carbon; f_a^{P}: aromatic ether or phenolic hydroxylcarbon; f_{al}: total aliphatic carbon; f_{al}^{*}: –CH_3; f_{al}^{H}: –CH or –CH_2; f_{al}^{O}: bonded to oxygen.

Table S6 The structure parameters of samples based on XRD and Raman.

Sample	d_{002} Å	L_c nm	L_a nm	R	A_D/A_G
NGC-HC	3.85	1.28	6.19	1.87	1.32
SGC-HC	3.80	1.51	6.56	2.53	1.22
LGC-HC	3.74	1.60	7.58	2.82	1.11

The carbon layer distance (d_{002}) was calculated based on Bragg's equation ($d = \lambda / 2\sin\theta$). The thickness ($L_c$) and average width ($L_a$) of graphite crystallites were calculated by Scherrer formula ($L = K\lambda/(\beta\cos\theta)$). The parameter ($R$), a representative measure calculated from the intensity of the (002) peak, which represents the ratio of the peak height to the background, has been used to quantify the degree of carbon disorder.

Table S7 The specific surface area, pore volume, and most probable apertures of samples based on N_2 adsorption-desorption test.

Samples	Surface Area ($m^2\ g^{-1}$)		Pore volume ($cm^3\ g^{-1}$)		Most probable apertures (nm)
	S_{BET}	S_{micro}	V_{total}	V_{micro}	
NGC-HC	17.7	10.2	0.02	0.005	2.0
SGC-HC	11.5	0	0.025	0	2.1
LGC-HC	13.3	0	0.024	0	1.9

Table S8 The pre-oxidation strategy for modifying pitch and the performance of SIBs

Samples	Modification Strategy	Gas/Liqued prooducts	Oxygen Content (wt%)	Capacity (mA h g^{-1}; mA g^{-1})	ICE (%)	Ref.
HPPC	HNO_3 oxidation; carbonized at 1300 °C	NO_3^-	-	317;30	88	1
CPOP	Air pre-oxidation at 300 °C; carbonized at 1400 °C	NO_x, SO_x, CO_2, Volatile Organic Compounds (VOC)	22	300; 30	88	2
HC-325-12	Air pre-oxidation at 325°C; carbonized at 1100 °C		28	300; 20	82	3
PAOC-300-10	Air pre-oxidation at 300°C; carbonized at 1200 °C		14	275;30	68	4
PHC-1300	HPO_4 modified at 360 °C-Air pre-oxidized at 320 °C; carbonized at 1400 °C	PO_4^-	-	284; 30	72	5
ACM-1400	HNO_3/H_2SO_4-oxidation at 80 °C; carbonized at 1400 °C	SO_4^{2-}、NO_3^-	-	292; 25	75	6
NGC-HC	H_2O_2/HCOOH-oxidation at 25 °C; carbonized at 1300 °C	H_2O	28	299; 30	73	work
SGC-HC	Oxidation-hydrothermal cascade strategy -	H_2O	18	318;30	76	This work

Table S9 The EIS fitting results for the samples by the equivalent circuit model.

Samples	R_e (Ω)	R_{SEI} (Ω)	R_{ct} (Ω)
NGC-HC	3.3	0.32	28.4
SGC-HC	3.4	0.22	18.3
LGC-HC	2.6	0.62	11.4
CTP-SC	2.9	0.90	4.3
S-OCTP-HC	2.9	0.80	13.2

1. Z. Xiong, L. Yue, Y. Zhang, H. Ding, L. Bai, Q. Zhao, T. Mei, J. Cao, Y. Qi and M. Xu, *Journal of Colloid and Interface Science*, 2024, **658**, 610-616.
2. Y. Lu, C. Zhao, X. Qi, Y. Qi, H. Li, X. Huang, L. Chen and Y.-S. Hu, *Advanced Energy Materials*, 2018, **8**, 1800108.
3. R. Xu, Z. Yi, M. Song, J. Chen, X. Wei, F. Su, L. Dai, G. Sun, F. Yang, L. Xie and C.-M. Chen, *Carbon*, 2023, **206**, 94-104.
4. B. Wang, Y. Yao, W. Wang, Y. Xu, Y. Wan, Y. Sun, Q. Li, H. Hu and M. Wu, *Journal of Colloid and Interface Science*, 2024, **664**, 681-690.
5. H. Wang, S. Liu, C. Lei, H. Qiu, W. Jiang, X. Sun, Y. Zhang and W. He, *Electrochimica Acta*, 2024, **477**, 143812.
6. Q. Li, Y. Zhu, P. Zhao, C. Yuan, M. Chen and C. Wang, *Carbon*, 2018, **129**, 85-94.